Origin of the fast photoresponse of epitaxial $YBa_2Cu_3O_{7-\delta}$ thin films

F. A. Hegmann
Department of Physics and Astronomy, McMaster University, Hamilton, Ontario, Canada L8S 4M1

J. S. Preston
Department of Engineering Physics, McMaster University, Hamilton, Ontario, Canada L8S 4M1

(Received 9 July 1993)

We have measured the photoresponse of current-biased bridge structures of epitaxial $YBa_2Cu_3O_{7-\delta}$ thin films on $LaAlO_3$ using 100 ps, 532 nm laser pulses. Voltage transients with fast and slow components were observed below T_c. The amplitude of the slow component agrees with a resistive bolometric response where the laser pulse heats the bridge into the resistive transition region. The decay time of the slow component is consistent with a thermal time constant for heat loss out of the film governed by the thermal boundary resistance at the interface between the film and the substrate. We show that the fast component can be explained by changes in the kinetic inductance of the bridge due to *temperature-induced* changes in the superfluid density from heating of the bridge by the laser pulse. Our interpretation of the origin of the fast component, therefore, is bolometric in nature over the time scale of the laser pulse contrary to some of the nonequilibrium or nonbolometric mechanisms that have been proposed. A simulation of this kinetic inductive bolometric effect provides reasonable agreement with the temperature dependence of the observed photoresponse, and a comparison is made between the various postulated temperature dependencies of the superfluid fraction in $YBa_2Cu_3O_{7-\delta}$. The simulation further shows that the speed of the kinetic inductive bolometric photoresponse is not limited by the thermal escape time out of the film, but is determined by the *rate* at which the incident laser pulse initially heats the film and is therefore the same duration in time as the laser pulse. Evidence for negative voltage transients observed in the photoresponse data consistent with the simulation results is also presented.

I. INTRODUCTION

The photoresponse of high-T_c superconductors has been actively studied over the past few years. The motivation behind most of the research has been the development of photodetectors sensitive to a very broad range of wavelengths. The ability to cool high-T_c superconducting films with liquid nitrogen has made them quite attractive for use as sensitive transition-edge bolometers.[1–4] Such detectors rely on heating from incident radiation inducing a large resistive change in the film biased in the sharp transition region. The response time of transition-edge bolometers is limited by the rate of heat loss out of the film, but thermal response times as short as 1 ns are possible.[5] Relatively well established with conventional superconductors, application of this technology with high-T_c superconductors has progressed to the point where one company[6] has marketed a superconducting bolometer for infrared detection using a patterned $YBa_2Cu_3O_{7-\delta}$ (YBCO) line on a micromachined silicon wafer.

Granular and epitaxial high-T_c thin films offer the possibility of developing very fast photodetectors which rely on nonequilibrium or nonbolometric (nonthermal) mechanisms for detection. Studying the nonbolometric photoresponse may also offer insight into the nature of superconductivity in the high-T_c oxides. The photoresponse in granular films[7–11] has been attributed to light-induced phase-slip processes in the Josephson junction weak links between the grains. Nanosecond response times have been observed in polycrystalline Tl-Ba-Ca-Cu-O thin films[10] at wavelengths larger than 100 μm, and response times of a few picoseconds have been predicted[11] in granular YBCO thin films.

It is not so clear that intergrain phase-slip processes can explain the fast photoresponse in epitaxial thin films characterized by high critical currents. Indeed there has been some controversy over whether or not high-T_c epitaxial thin films exhibit a nonbolometric photoresponse at all. In some experiments, only a bolometric photoresponse in epitaxial thin films was observed[12–14] where the voltage transients could be explained by the laser pulses heating the film within or into the resistive region. In other experiments, both bolometric and nonbolometric signals were observed,[15–25] where bolometric usually implied a resistive mechanism and nonbolometric was a term used by many authors to refer to signals that were too fast or had too little temperature dependence below T_c to be due to the resistive bolometric mechanism.[15] While in some cases, nanosecond thermal transients may have been misinterpreted as nonbolometric transients,[5] the 30 ps wide voltage transients recently observed[25] in epitaxial YBCO thin films cannot be explained by characteristic thermal response times.

Nonbolometric signals have also been identified by deviations of the observed transient voltage ΔV from a simple resistive bolometric response governed by $\Delta V = I\, dR/dT\, \Delta T$, where I is the bias current, dR/dT is the temperature derivative of the resistance, and ΔT is

the transient temperature generated in the film by the incident light. It should be noted that this approach is invalid for the large ΔT produced by intense laser pulses since the resistance curve of a superconductor is highly nonlinear near T_c. Using the actual $R(T)$ is preferred; however, precise values of ΔT are required to make a clear and unambiguous identification of a nonthermal photoresponse which relies on accurate thermal modeling.[5,26,27] A magnetic field has been used in a technique to help distinguish between bolometric and nonbolometric components in the photoresponse of epitaxial YBCO thin films.[28]

Among the groups that have reported a nonbolometric photoresponse, there has been little consensus regarding the origin of the nonbolometric mechanism in epitaxial thin films. The nonbolometric photoresponse has been discussed in terms of optically generated quasiparticles suppressing the superconducting order parameter[16–18,20,22–24,33] or changing the sample's kinetic inductance,[16,18–20,23,25] or attributed to optically induced flux motion phenomena such as photoenhanced flux creep,[29] photoactivated flux flow,[17] and photofluxonic detection.[30] Fast current switching of optically thick YBCO films by intense laser pulses[31] was explained by nonequilibrium hot electrons inducing a bolometric response after having traveled to the back of the film. A related set of experiments involves pump-probe measurements of YBCO thin films which have examined quasiparticle thermalization times,[32–35] electron-phonon coupling parameters,[36] and quasiparticle recombination times[32] over subpicosecond and picosecond time scales. However, interpretation of the results from these experiments remains controversial.[37]

In this paper, we argue that the fast photoresponse observed below T_c in epitaxial YBCO thin-film bridge structures due to 100 ps laser pulses, which we previously attributed to a nonbolometric mechanism,[28] can be explained by temperature-induced changes of the kinetic inductance in the bridge and is, therefore, essentially bolometric in origin. Kinetic inductance arises from the inertia of the superconducting electrons and, as discussed later, is inversely proportional to the superfluid density (or proportional to λ_L^2, where λ_L is the London penetration depth). The superfluid density depends on temperature, so the temperature transient induced by the laser pulse will change the kinetic inductance of the bridge. At constant current bias, a change in kinetic inductance will produce a voltage transient across the bridge which constitutes the photoresponse. The voltage transient is potentially the same width as the laser pulse, or 100 ps in this case. However, bandwidth limitations in the measuring circuit (see Sec. II) have limited the observed widths to just under 500 ps. The fast component can therefore be described as a kinetic inductive bolometric response. Slower components in the photoresponse with nanosecond decay times observed near the transition region are due to a resistive bolometric response.

The study of kinetic inductance in superconductors is not a new subject. The kinetic inductance of microwave superconducting microstrip transmission lines has been studied extensively.[38] The temperature variation of the kinetic inductance has been used in YBCO microstrip resonators to measure the temperature dependence of the London penetration depth[39] (providing information on the superfluid fraction) and in variable delay YBCO microstrip delay lines.[40] Recently, an optically modulated superconducting delay line has been constructed which relies on the bolometric modulation of the kinetic inductance in a YBCO microstrip.[41] Kinetic inductance bolometers have also been developed[42] which operate below T_c and require a superconducting quantum interference device (SQUID) to sense changes in the inductance of the circuit. The kinetic inductive bolometric mechanism we are proposing for the fast photoresponse is similar to the detection principle of a kinetic inductance bolometer. To our knowledge, this is the first time such a mechanism has been used to explain the origin of the fast photoresponse in high-T_c epitaxial thin films.

The remainder of the paper is organized as follows. The YBCO film characteristics and photoresponse measurement techniques are discussed in the Sec. II. Section III discusses the broadening of the resistive transition due to the bias current, shows some typical transient voltage wave forms, describes the temperature and current dependence of the photoresponse, and analyzes the resistive bolometric response due to heating from the laser pulse in the transition region. The origin of the fast photoresponse is discussed in terms of kinetic inductance, and a simulation of the photoresponse based on the kinetic inductive bolometric response mechanism is compared with our observations. Finally, a summary is given in Sec. IV.

II. EXPERIMENT

Epitaxial thin films of YBCO were deposited on $LaAlO_3$, substrates by laser ablation. The c-axis films were grown at 760 °C in 300 mTorr oxygen, then allowed to cool in 0.5 atm oxygen. Film thickness ranged from 30 to 260 nm, and substrate sizes were nominally $6\times6\times0.5$ mm^3. The films were patterned into bridge structures using standard photolithographic techniques and a wet chemical etch of 0.1% HCl and HNO_3 in deionized water. Etch times were typically 10–20 s, thus minimizing the exposure time of the films in water. Standard lift-off techniques were used to pattern 200-nm-thick gold pads on the YBCO film. Contact resistance was less than 0.1 Ω after annealing at 500 °C for 30 min in 1 atm flowing oxygen. The annealing process also improved the adhesion of the gold pads to the YBCO film.

Table I gives the characteristics after processing for the four films described here. The zero resistance critical temperature T_{c0} ranged from 86 to 90 K, and transition widths ΔT_c varied from 3 K for the thinnest film to about 1 K for the thickest films. Degradation of T_{c0} due to processing was about 2 K for the thinnest films and less than 0.5 K for the thickest films. In particular, the 30 nm film degraded further in time as a result of oxygen loss from the bridge. The critical current density J_c for the bridges at 77 K was nominally 1×10^6 A/cm^2 after processing, using a voltage criteria of 10^{-7} V across the 200 μm bridges or 5 μV/cm. Bridge resistivities were typically

TABLE I. Specifications for the four films described in the paper. The patterned bridges have a thickness d, width w, and length l. $T_{c0(R=0)}$ is the zero resistance transition temperature after patterning using a 10^{-7} V criteria (5 μV/cm), and ΔT_c is the width of the superconducting transition. The critical current I_c at 77 K (5 μV/cm criteria) for each bridge is shown from which the critical current density J_c at 77 K is calculated. The resistance R of the bridge at 100 K is used to estimate the corresponding resistivity ρ. When referring to a specific film in the text, the film thickness d will be used.

d (nm)	w (μm)	l (μm)	$T_{c0(R=0)}$ (K)	ΔT_c (K)	I_c at 77 K (mA)	J_c at 77 K (A/cm^2)	R at 100 K (Ω)	ρ at 100 K ($\mu\Omega$ cm)
30	20	200	86	3	5	8.3×10^5	600	180
130	20	200	87	2	25	9.6×10^5	120	160
220	20	200	90	<1	100	2.3×10^6	50	110
260	10	200	89	1	45	1.7×10^6	110	140

150 $\mu\Omega$ cm at 100 K.

A frequency doubled Nd:YAG laser provided 100 ps, 532 nm (2.33 eV) mode-locked pulses at a repetition rate of 76 MHz. The 1.5 W average laser power from this source resulted in excessive sample heating and made photoresponse measurements difficult. In order to maintain a high energy per pulse but lower the average power in the beam, a pulse extraction system was used to select individual pulses at a repetition rate of 12.7 kHz. This lowered the average beam power at the sample to less than 0.4 mW while providing 4 nJ per selected pulse. The contrast ratio of the pulse selection system was typically 300:1. Variations in the contrast ratio had little effect on the amplitude of the selected pulse, but had a large effect on the average beam power. It was estimated that the average beam power of 0.4 mW increased the temperature of the sample by less than 0.1 K. Power dissipation at the current contacts was at most about 1 mW and therefore did not contribute significantly to heating of the sample. A cylindrical lens was used to focus the laser pulse to a 20 μm$\times$200 μm elliptical spot on the bridge, producing a fluence of about 100 μJ/cm^2. The long axis of the spot was oriented perpendicular to the bridge to minimize beam misalignment due to thermal drift of the sample holder in the chamber.

The samples were mounted in vacuum on the end of a cold finger of a closed cycle He gas refrigerator. The measuring circuit is shown in Fig. 1. A constant current source provided bias currents up to 100 mA through two of the four gold contacts on the YBCO film. The other two contacts were connected to a 50 Ω SMA coaxial cable 40 cm long which brought the transient voltage signal from the bridge structure to a bias T and amplifier. The bias T had a rise time of 20 ps and a lower cutoff of 0.5 MHz. The amplifier, which had a gain of 20 dB ($\times$10 voltage gain) from 0.1 MHz to 1 GHz, enabled low level transients to be observed on a 20 GHz sampling oscilloscope, resulting in a system rise time of 400 ps. We did observe photoresponse transients with full widths at half maximum (FWHM) less than 500 ps, but we assume these were attenuated due to the finite frequency response of our circuit. A nanovoltmeter attached to the bias-T allowed *in situ* four-point probe voltage measurements across the bridge with a resolution of 50 nV. Each wave form acquired on the sampling oscilloscope was averaged 128–512 times. Wave forms were taken at positive and negative current bias and then subtracted to remove dc offsets and noise pickup, resulting in a noise limit on the wave forms acquired from the oscilloscope of about 0.05 mV.

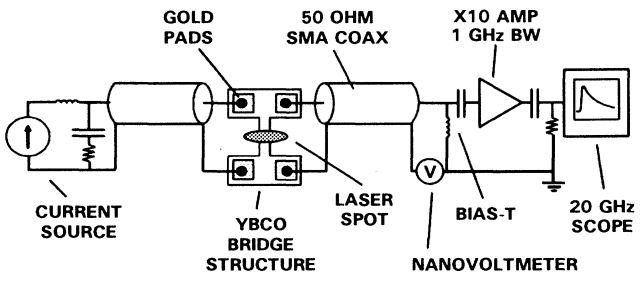

FIG. 1. Schematic of the experimental setup used for the photoresponse measurements.

III. RESULTS

A. Broadening of the resistive transition due to bias current

Before photoresponse measurements on a sample were taken, the steady state (dc) voltage across the bridge was plotted as a function of temperature and various bias currents, as shown in Fig. 2(a) for the 260 nm film. This provided a detailed "map" of the resistive transition region which enabled identification of the resistive bolometric photoresponse. As the current bias increased, the value for T_{c0} decreased (10^{-7} V criteria) and the width of the transition increased. The critical current I_c is a linear function of temperature from 65 to 85 K, which is consistent with the temperature dependence of the critical current density J_c observed in YBCO thin films.[43] With the bias current held constant, increasing the temperature beyond a certain point resulted in a very sharp and sudden upturn in the measured voltage which may have been due to runaway thermal effects from the generation of hot spots in the bridge.[44] Figure 2(b) plots the resistance of the bridge as a function of temperature and bias current on a linear scale to emphasize the broadening. Several photoresponse studies[12,17,28,29] have

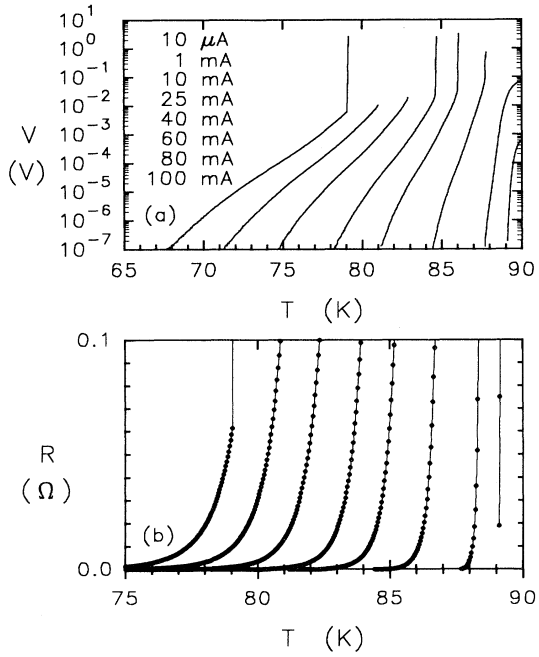

FIG. 2. Resistive transition broadening as a function of bias current observed for the 260 nm film under steady-state (dc) conditions and zero external field. In (a), the dc voltage V measured across the 200 μm long bridge is plotted on a logarithmic scale as a function of temperature T. The rightmost curve is for a bias current of 10 μA, and the leftmost curve with the broadest transition was taken at 100 mA. The corresponding bridge resistance R is plotted on a linear scale in (b) as a function of temperature to emphasize the broadening of the transition and lowering of T_{c0} due to the bias current. The lines drawn in (b) are only guides to the eye. Similar plots were made for the other films providing maps of the resistive transitions for each film.

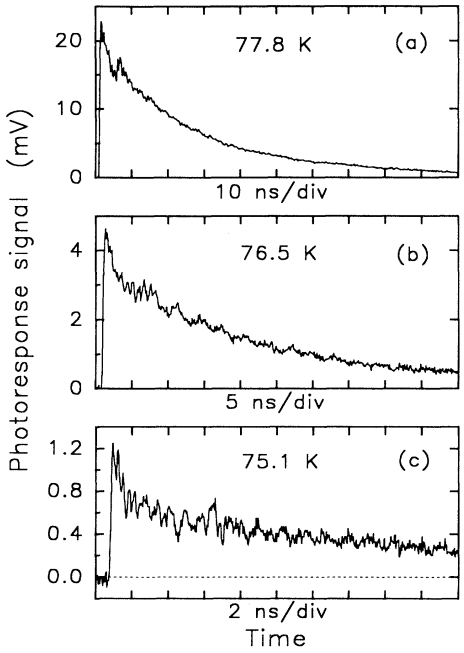

FIG. 3. Photoresponse signals observed in the resistive transition region of the 260 nm film at a bias of 100 mA and laser fluence of 100 μJ/cm^2. Notice the change in the time scale for each of the wave forms. In (a), at a temperature of 77.8 K, the signal is quite large and has a long decay. As the temperature is lowered to 76.5 K in (b), the slowly decaying component has decreased dramatically in amplitude, but a fast component begins to appear at the start of the wave form. In (c) at 75.1 K, the fast component is becoming more prominent and the slow component has decreased further in amplitude.

examined the effect of current bias on the resistive transition.

Considering that only 20 μm of the 200-μm-long bridge was illuminated by the laser spot and the amplifier had a gain of 10, it was possible to use the resistive transition map for each sample to directly convert observed voltage transients to transient temperatures if the photoresponse was resistive bolometric in origin. Examples of this method are discussed in the next section and more thoroughly in Sec. III E.

B. Typical photoresponse wave forms

The observed transient voltages for the 260 nm film with 100 mA bias are shown in Figs. 3 and 4 for various temperatures. Figure 5 shows an expanded view of the 100 mA resistive transition curve from Fig. 2(a). Figure 3(a) shows the transient response of the bridge at a temperature of 77.8 K which is close to the sudden upturn seen in Fig. 5(a) at 79 K. The amplitude of the signal is large and the decay time is close to 30 ns. As the temperature is lowered to 76.5 and 75.1 K, a fast transient peak appears at the start of the slowly decaying component as shown in Figs. 3(b) and 3(c). In Fig. 4(a), the fast component dominates over slow component at 74.2 K, and in Fig. 4(b) the slow component has completely vanished below our noise limit at 71.4 K and all that remains is the fast component with a pulse width less than 500 ps. The fast component persists with decreasing amplitude even to lower temperatures. This is shown in Fig. 4(c) where the temperature has been reduced to 45.7 K.

We will show that the temperature transient induced by the laser pulse in the current-biased bridge produces two types of photoresponse: (1) a slow component due to a resistive bolometric photoresponse which dominates when the maximum temperature attained by the temperature transient in the bridge is within the resistive transition region, and (2) a fast component due to a kinetic inductive bolometric photoresponse which can be seen at temperatures below the resistive transition. Photoresponse signals consisting of a fast component followed by a slow component have been reported by other groups studying the photoresponse of epitaxial YBCO thin films.[15,18,20–23,25,45]

The resistive transition curve shown in Fig. 5 can be used to determine the resistive bolometric nature of the slow component and demonstrate the nonresistive nature of the fast component.[28] In Fig. 3(b), the amplitude of

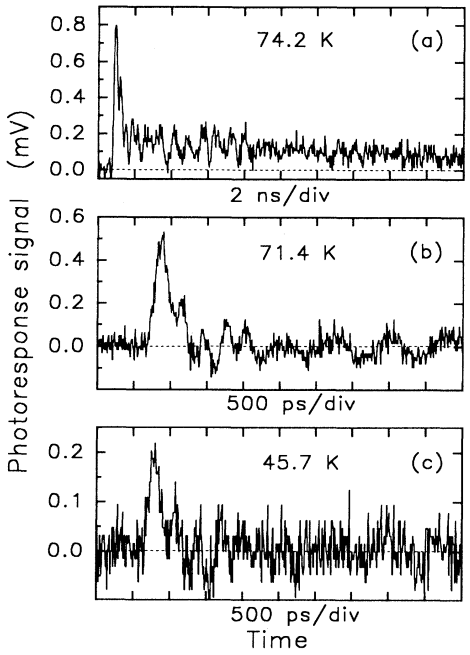

FIG. 4. Photoresponse signals observed in the resistive transition region and at lower temperatures for the 260 nm film at a bias of 100 mA and laser fluence of 100 $\mu J/cm^2$. The sequence of wave forms presented here is continued from Fig. 3. Notice the change in time scale for the wave forms. In (a), at a temperature of 74.2. K, the fast component at the start of the wave form dominates over the slow component. At 71.4 K in (b), the slow component has completely disappeared below the noise level of the oscilloscope and only the fast component remains. The fast component persists to lower temperatures with a decreased amplitude as shown in (c) at a temperature of 45.7 K well below the resistive transition region. The fast photoresponse in (c) is less than 500 ps wide.

the slow component is roughly 3.5 mV. At an initial temperature $T_{INITIAL}$ of 76.5 K, Fig. 5(b) indicates that the initial dc voltage across the bridge is about 0.4 mV. Since the sample is ac coupled to the scope, a voltage transient ΔV of 3.5 mV due to a change in resistance of the bridge produces a maximum voltage across the bridge of 3.9 mV, which corresponds to a maximum temperature T_{MAX} of 78.7 K in Fig. 5(b) or a temperature transient ΔT of 2.2 K. From the analysis given in Sec. III E below, a simple thermal model provides an estimate of 3.4 K for the temperature transient, which is close to the observed value in this case of 2.2 K. Interpreting the 0.2 mV fast response seen at 45.7 K in Fig. 4(c) to a change in resistance of the bridge would require a transient temperature of almost 30 K according to Fig. 5. This is quite different from a 7.8 K transient predicted by the simple thermal model, implying that the fast response cannot be due to a resistive bolometric effect. The fact that the fast response can be explained by kinetic inductance effects will be demonstrated by a simulation of the photoresponse data given in Sec. III F.

C. Temperature dependence of the photoresponse

The amplitude of the photoresponse as a function of temperature and at a constant bias current for the 260 nm film is shown in Fig. 6. Examples of wave forms observed in this temperature range are shown in Figs. 3 and 4. The rapid decrease of the signal as the temperature is lowered below the resistive transition region is evident. However, the photoresponse is seen to persist to lower temperatures. The inset of Fig. 6 shows more clearly the amplitude of the fast and slow components as a function of temperature below the resistive transition. Notice how the slow component, which is attributed to resistive bolometric effects, disappears quite sharply below the resistive transition region. Below 72 K, the slow component has completely vanished and only the fast component remains which decreases more slowly in amplitude as the temperature is lowered further.

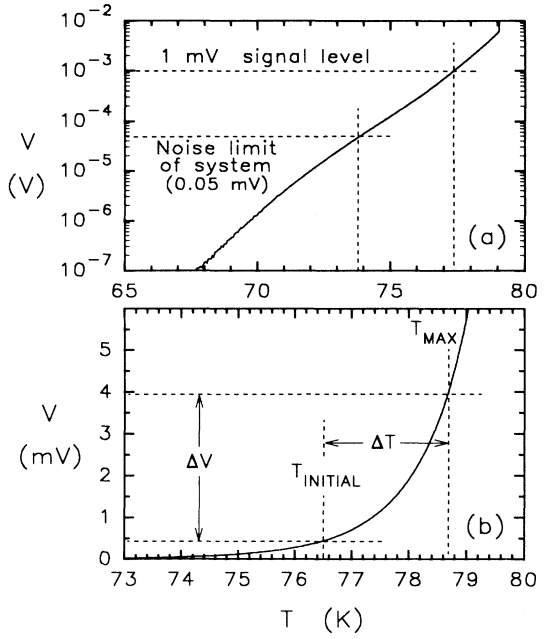

FIG. 5. Expanded view of the dc voltage V measured across the 200-μm-long bridge as a function of temperature for the 260 nm film at a bias of 100 mA taken from Fig. 2(a). The curve can be used to determine if the observed photoresponse was due to temperature transients induced by the laser pulse bringing the temperature of the bridge into the resistive region. In (a), the noise limit of 0.05 mV determines the minimum temperature ($\approx$73.8 K) needed to be reached at the peak of the temperature transient in the film in order for a resistive photoresponse to be observed. In other words, resistive bolometric voltage transients would not be seen on the oscilloscope if this minimum temperature requirement were not satisfied. If the peak temperature reached by the film were around 77.3 K and the initial temperature was less than 70 K, then the resistive photoresponse signal would be about 1 mV. The transition curve is plotted on a linear scale in (b). The parameters shown in (b) are described in the text.

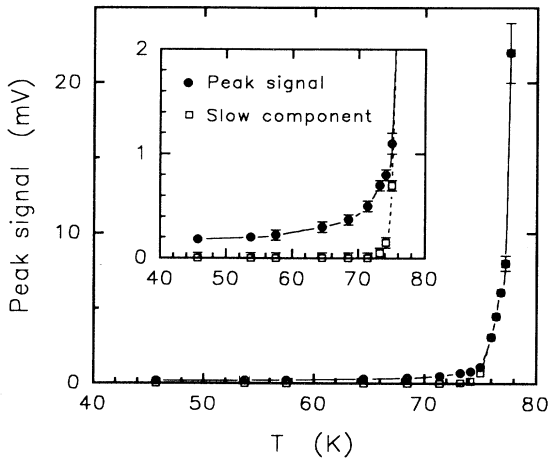

FIG. 6. Temperature dependence of the peak photoresponse signal for the 260 nm film at a bias of 100 mA and laser fluence of 100 μJ/cm^2. Examples of some of the wave forms for these points are shown in Figs. 3 and 4. The inset shows the low-temperature region more clearly and plots the peak amplitude of the photoresponse signal (filled circles) and the amplitude of the slow component only (open squares) which follows the fast transient. The slow component rapidly disappears as the temperature is lowered, and only the fast component remains at temperatures less than 72 K. The lines are a guide to the eye.

D. Current dependence of the photoresponse

Figure 7 shows the amplitude of the photoresponse signal as a function of current bias for the 260 nm film at a constant temperature of 78 K. Figure 8 shows typical wave forms associated with the data points in Fig. 7. The

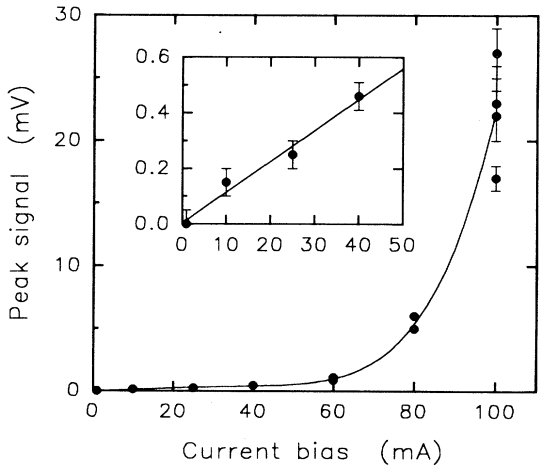

FIG. 7. Bias current dependence of the peak photoresponse signal for the 260 nm film at a temperature of 78 K and laser fluence of 100 μJ/cm^2. The inset shows the linear dependence of the photoresponse with bias current at low current values. In the linear regime, only the fast photoresponse is observed. The sudden increase in signal amplitude seen above 60 mA is due to the film entering the resistive region at these higher current levels. The line in the main plot is only a guide to the eye. The line in the inset is a linear regression fit to the low current data. Examples of some of the wave forms for these points are shown in Fig. 8.

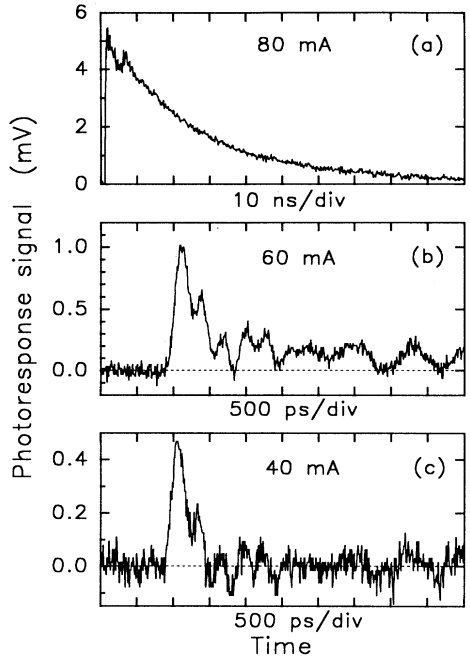

FIG. 8. Bias current dependence of the observed photoresponse wave forms for the 260 nm film at a temperature of 78 K and a laser fluence of 100 μJ/cm^2. Notice the change in time scale for the wave forms. The amplitudes of these transients are plotted in Fig. 7. At high bias currents, the signal is resistive bolometric and has a long decay time as shown in (a). As the current is lowered to 60 mA in (b), the slow component is almost gone. Only the fast component remains in (c) since a bias of 40 mA is insufficient to bring the film into the resistive region. Below 40 mA, the amplitude of the fast response is linear with current, as shown in the inset of Fig. 7.

sudden rise in amplitude of the photoresponse above 60 mA corresponds to the induced temperature transient entering the broadened resistive region at higher bias currents, as can be seen by examining Fig. 2(a). The scatter in the peak signal readings at 100 mA in Fig. 7 is due to small changes in laser fluence near the highly nonlinear upturn of the resistive transition shown in Fig. 5. A slow component in the photoresponse was observed for currents above 60 mA, as shown in Fig. 8(a) at 80 mA and Fig. 8(b) at 60 mA. Below 60 mA, which was out of the resistive transition region, only a fast photoresponse was observed, as seen in Fig. 8(c) for a 40 mA bias. What is important to note here is that the fast photoresponse observed below 60 mA varied *linearly* with current, as shown more clearly in the inset of Fig. 7. A linear dependence of the fast photoresponse with bias current has also been observed elsewhere.[17–19,23,24]

Similar behavior in the photoresponse was also seen in the 30 nm film, as shown in Fig. 9, and the 130 and 220 nm films. Figure 10 shows wave forms for some of the data points in Fig. 9. The voltage transient seen in Fig. 10(a) for the 30 nm film at a bias of 60 mA is a resistive bolometric response with a width of about 650 ps

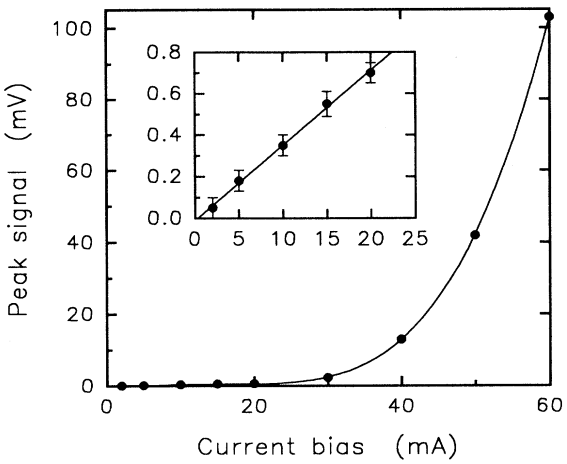

FIG. 9. Bias current dependence of the peak photoresponse signal for the 30 nm film at a temperature of 54 K and laser fluence of 100 μJ/cm^2. The inset shows the linear dependence of the photoresponse with bias current at low current values. As in Fig. 7 for the 260 nm film, only the fast photoresponse was observed in this linear regime. The line in the main plot is only a guide to the eye. The line in the inset is a linear regression fit to the low current data. Examples of some of the wave forms for these points are shown in Fig. 10.

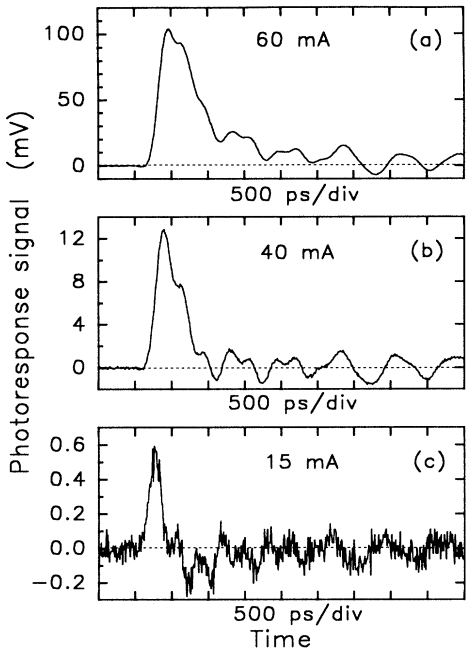

FIG. 10. Bias current dependence of the observed photoresponse wave forms for the 30 nm film at a temperature of 54 K and a laser fluence of 100 μJ/cm^2. The amplitudes of these transients are plotted in Fig. 9. The fast, 650 ps FWHM transient with 60 mA bias seen in (a) is a resistive bolometric response. In (b) at 40 mA, the film is still in the resistive region and the response is still resistive bolometric despite its 450 ps FWHM pulse width. The film leaves the resistive region for currents below 30 mA and only the fast response is seen, as shown in (c) at a bias of 15 mA. In this current region, the fast photoresponse is linear with bias current, as shown in the inset of Fig. 9.

FWHM. Reducing the current to 40 mA in Fig. 10(b) produces a transient still in the resistive region with a width of about 450 ps FWHM. In Fig. 10(c), the current level is low enough to bring the film out of the resistive transition region, and the amplitude of the fast response is linear with current, as shown in the inset of Fig. 9. The width of the transient in Fig. 10(c) is about 220 ps FWHM. As mentioned earlier, the amplitude of these short transients will be attenuated due to the finite bandwidth of the measuring circuit.

E. Analysis of the resistive bolometric (slow) photoresponse

Examples of resistive bolometric wave forms from the four films at temperatures and bias currents in the resistive transition region are shown in Fig. 11. The decay time of the voltage transients decreases as the film thickness is reduced. This is consistent with faster thermal decay times for thinner films, but the magnitude of the thermal escape time cannot be read directly from the voltage transient wave forms due to the nonlinearity of the resistive transition. The temperature transient as a function of time induced in the film by the laser pulse can be determined by finding the temperature in the dc resistance transition curve at which the dc voltage equals the voltage in the photoresponse transient at a given time.

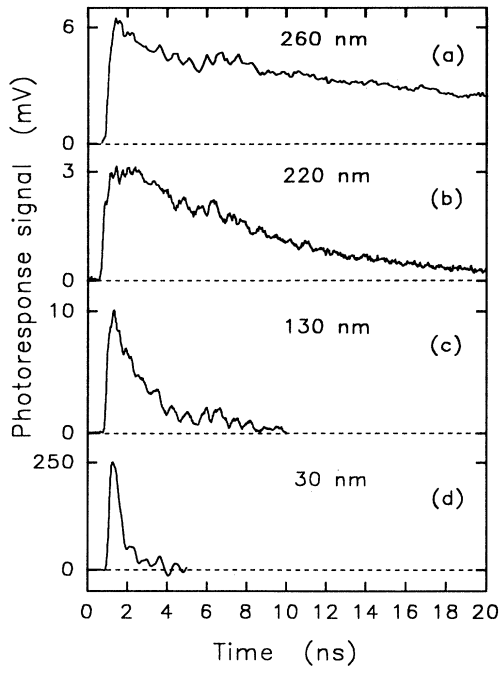

FIG. 11. Examples of resistive bolometric photoresponse signals seen in the four films biased in their resistive transition regions. The decay time for the 260 nm film in (a) is greater than 20 ns, but gets progressively shorter as the film thickness is decreased becoming as short as 1 ns for the 30 nm film in (d). The temperature at which each of the wave forms was taken is given in Table II. The laser fluence was 100 μJ/cm^2, and the current bias was 100 mA in (a), 80 mA in (b), 75 mA in (c), and 20 mA in (d).

An example of this technique, which gives more accurate estimates of thermal escape times, is described below.

A voltage transient from the 130 nm film at 70 K is shown in Fig. 12. A current of 75 mA was enough to bias the bridge into the resistive transition region, as seen in Fig. 13. The temperature transient shown in Fig. 12 was obtained by converting the voltage transient values in Fig. 12 to equivalent temperatures using Fig. 13. Due to the nonlinear nature of the resistive transition, the decay of the transient voltage signal is much faster than the decay of the temperature transient. The same technique was used on the resistive bolometric signals from the other films shown in Fig. 11, and the normalized temperature transients are shown in Fig. 14. The main feature of Fig. 14 is the faster thermal decay observed for thinner films. The amplitudes and thermal decay times (exponential fit) of the observed temperature transients for the four films are given in Tables II and III, respectively.

A simple thermal model using the thermal boundary resistance between the film and the substrate[5] can be used to estimate the amplitude of the transient temperature

$$\Delta T_{\text{ESTIMATE}} = \frac{F}{Cd}\frac{E_{\text{ABS}}}{E_0} \tag{1}$$

and the thermal decay time for heat loss out of the film

$$\tau_{\text{ESTIMATE}} = CR_{\text{BD}}d \ , \tag{2}$$

where F is the incident laser fluence in J/cm^2, C is the heat capacity of the film in J/cm^3 K, d is the thickness of the film in cm, and R_{BD} is the thermal boundary resistance in K cm^2/W. The factor E_{ABS}/E_0 is the fraction of the total incident energy absorbed in the film and takes into account transmission of the laser pulse through the film and reflection from the front surface given by

$$E_{\text{ABS}}/E_0 = (1-R)[1-\exp(-d/\delta)] \ , \tag{3}$$

where R is the reflectivity and δ is the optical penetration depth. Equation (3) neglects reflection from the back surface of the film and multiple reflections in thin films.

The heat capacity[46,47] of YBCO decreases almost

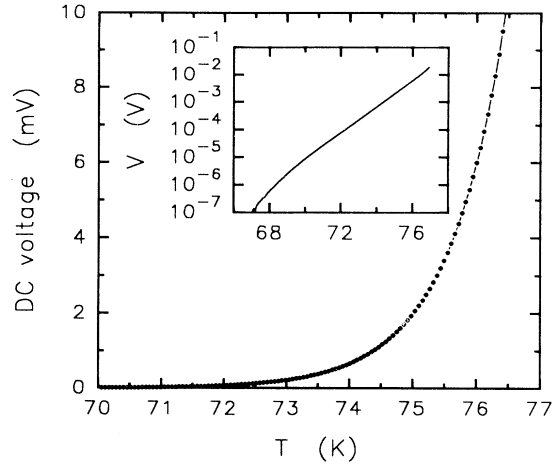

FIG. 13. dc voltage measured across the 200-μm-long bridge as a function of temperature for the 130 nm film at a bias of 75 mA. This curve was used to determine the temperature transient induced in the film shown in Fig. 12. The line is a guide to the eye. The inset plots the voltage on a logarithmic scale showing an exponential voltage dependence over most of the temperature range for this sample.

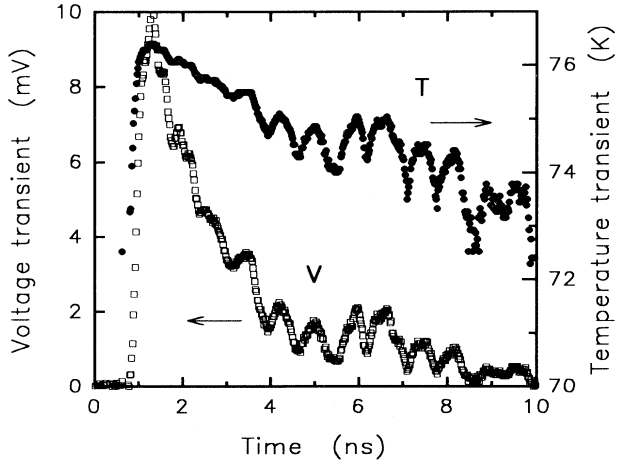

FIG. 12. Voltage transient (V, open squares) observed from the 130 nm film biased in the resistive transition region (T=70 K, I=75 mA, F=100 μJ/cm^2) and corresponding temperature transient (T, closed circles) interpolated from the measured dc resistive transition curve shown in Fig. 13. Due to the nonlinear nature of the resistive transition, the voltage transient has a faster fall time than the temperature transient. The voltage transient is the same as that shown in Fig. 11(c).

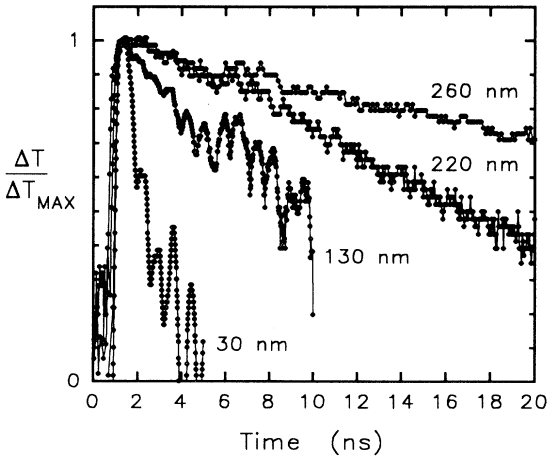

FIG. 14. Normalized temperature transients interpolated from photoresponse signals (shown in Fig. 11) taken in the resistive transition regions of the four films. As discussed in the text, the faster thermal decay time observed for the thinner films is consistent with Eq. (2). Exponential fits to this data provided values for the maximum temperature transients ΔT_{MAX} and thermal decay times τ_{OBSERVED} for each of the films, as shown in Tables II and III.

linearly from a value of 1.0 J/cm^3 at 78 K to 0.4 J/cm^3 at 45 K (see Fig. 16 in Sec. III F). The thermal boundary resistance[5] between YBCO thin films and $LaAlO_3$ substrates is nominally 1.0×10^{-3} K cm^2/W and independent of temperature from 90 to 200 K. At lower temperatures,

$$R_{BD}=B/T^3 , \tag{4}$$

where $B\approx17$ K^4 cm^2/W for YBCO on sapphire.[5] Therefore, the T^{-3} behavior of R_{BD} will become significant for temperatures below 30 K, and will have the effect of increasing the thermal escape time from the film. At 532 nm (2.33 eV), the reflectivity[48] of bulk single-crystal YBCO is about 10% ($R=0.1$), and the absorption coefficient α of YBCO thin films[49] is approximately 1.1×10^5 cm^{-1} which gives an optical penetration depth of $\delta=1/\alpha\approx90$ nm. Using Eq. (3), E_{ABS}/E_0 will be 0.85 for the 260 nm film and 0.26 for the more transmissive 30 nm film. If a shorter optical penetration depth[50] of 60 nm at 532 nm is used, the values for E_{ABS}/E_0 change to 0.89 and 0.35, respectively, which will not seriously affect the results. However, even though the thinner film absorbs less energy from the laser pulse, the temperature transient induced in the thinner film will be larger. As an example, if the laser fluence is 100 μJ/cm^2 and the heat capacity is 1.0 J/cm^3 K ($T=78$ K), then from Eq. (1) we find that ΔT induced by the laser pulse is 3.3 K for the 260 nm film and as high as 8.7 K for the 30 nm film. From Eq. (2), the thermal escape times will then be 26 ns for the 260 nm film and only 3 ns for the 30 nm film at 78 K.

Table II compares the transient temperatures extracted from the analysis above to estimates of ΔT using Eq. (1). The agreement is within a factor of 2, which is reasonable considering the uncertainty in some of the parameters. The agreement is also quite reasonable in Table III when comparing estimates of the thermal escape time using Eq. (2) to exponential fits of the decay times for the observed temperature transients shown in Fig. 14. If it is not assumed that $R_{BD}=1.0\times10^{-3}$ K cm^2/W (Ref. 5), then R_{BD} can be estimated using the observed thermal decay times. The average value of the estimates for R_{BD} given in Table III is $(1.1\pm0.6)\times10^{-3}$ K cm^2/W, which is in good agreement with other reported values.[5,14,23,51] This

TABLE II. Comparison of observed transient temperature amplitudes $\Delta T_{OBSERVED}$ for the four films of thickness d to estimates of the transient temperature $\Delta T_{ESTIMATE}$ using Eq. (1). The estimates use the heat capacity C of the YBCO film at an initial temperature T_i. E_{ABS}/E_0 is the fraction of incident laser pulse energy absorbed in the film, as described by Eq. (3). ($F=100$ μJ/cm^2, $R=0.1$, $\delta=90$ nm.)

d (nm)	T_i (K)	C (J/cm^3 K)	E_{ABS}/E_0	$\Delta T_{OBSERVED}$ (K)	$\Delta T_{ESTIMATE}$ (K)
30	73	0.91	0.26	~5	9.5
130	70	0.85	0.69	6.3	6.2
220	84	1.11	0.82	1.7	3.4
260	77	0.98	0.85	2.3	3.3

analysis supports the claim that the slow component is a resistive bolometric photoresponse with a decay time determined by the thermal boundary resistance between the YBCO film and the $LaAlO_3$ substrate.

We now consider characteristic thermal diffusion times given by

$$\tau_{DIFF}=\frac{d^2}{D}=\frac{d^2C}{\kappa} , \tag{5}$$

where D is the thermal diffusivity in cm^2/s and κ is the thermal conductivity W/cm K. Using τ_{DIFF} as an estimate for the rate of heat loss out of the film and into the substrate would assume that there is no thermal mismatch at the boundary between the YBCO film and the $LaAlO_3$ substrate. Values for κ in YBCO single crystals[52] depend on sample quality and direction of heat flow[53] but are nominally 0.12 W/cm K in the ab plane near 80 K and roughly 4 to 5 times smaller[53] along the c axis. This would give $D_{ab}\approx0.12$ cm^2/s and $D_c\approx0.026$ cm^2/s near 80 K. Since the epitaxial films used here have the c axis perpendicular to the substrate, we consider the thermal diffusivity along the c axis for heat flow out of the film and into the substrate. Upper estimates for τ_{DIFF} along the c axis are shown in Table III using Eq. (5) with $\kappa_c\approx0.026$ W/cm K and $C\approx1$ J/cm^3 K. For the thinnest films, a thermal boundary resistance model is in better agreement with the data. Thermal diffusion time constants will become significant in thicker films since the incident light is absorbed mainly in the first 100 nm of the film thickness.

F. Discussion of the origin of the fast photoresponse

1. Kinetic inductance interpretation

Under dc bias, a superconductor will ideally exhibit zero resistance. If an alternating bias is supplied, a finite voltage will appear across the superconductor due to the inertia of the superconducting carriers. The kinetic inductance, which gives rise to this impedance in the superconductor, for a superconducting strip of length l, width w, and thickness d can be expressed[38] in several ways as

$$L_{KIN}=\frac{m}{n_{SC}e^2}\left[\frac{l}{wd}\right]=\mu_0\lambda_L^2\left[\frac{l}{wd}\right]$$
$$=\frac{1}{\varepsilon_0\omega_{P_{SC}}^2}\left[\frac{l}{wd}\right]=\frac{1}{\varepsilon_0\omega_P^2}\left[\frac{1}{f_{SC}}\right]\left[\frac{l}{wd}\right] \tag{6}$$

where m is the effective mass of the superconducting carriers, n_{SC} is the density of superconducting carriers in a two fluid model, μ_0 is the permeability of free space, ε_0 is the permittivity of free space, λ_L is the temperature-dependent London penetration depth, ω_P is the plasma frequency, and f_{SC} is the superfluid fraction equal to n_{SC}/n, where n is the total density of carriers. The kinetic inductance of a superconducting bridge is therefore proportional to the square of the London penetration depth or inversely proportional to the superfluid fraction. The forms with λ_L and ω_P in Eq. (6) are useful in that λ_L and ω_P can be determined more accurately than n_{SC} or

TABLE III. Comparison of observed thermal decay times τ_{OBSERVED} for the four films of thickness d to estimates τ_{ESTIMATE} of the thermal decay time using Eq. (2) with the heat capacity C at an initial temperature T_i and a thermal boundary resistance of $R_{\text{BD}}=1.0\times10^{-3}$ K cm^2/W (Ref. 5). An exponential fit to the observed temperature transients shown in Fig. 14 for the four films is used to determine the thermal decay times τ_{OBSERVED}. $R_{\text{BD ESTIMATE}}$ is obtained using the observed decay times in Eq. (2), giving an average value for R_{BD} of about $(1.1\pm0.6)\times10^{-3}$ K cm^2/W. τ_{DIFF} is an estimate of the thermal diffusion time along the c axis as discussed in the text using Eq. (5).

d (nm)	T_i (K)	C (J/cm^3 K)	τ_{OBSERVED} (ns)	τ_{ESTIMATE} (ns)	$R_{\text{BD ESTIMATE}}$ (K cm^2/W)	τ_{DIFF} (ns)
30	73	0.91	1.5	2.7	5.5×10^{-4}	0.31
130	70	0.85	12	11	1.1×10^{-3}	5.5
220	84	1.11	18	24	7.4×10^{-4}	21
260	77	0.98	52	25	2.0×10^{-3}	25

m. A laser pulse absorbed in the superconductor will break Cooper pairs and reduce the superfluid fraction from its initial value, thereby increasing the kinetic inductance.

The superfluid current density is given by

$$J_{\text{SC}}=n_{\text{SC}}ev_{\text{SC}}\ , \tag{7}$$

where v_{SC} is the velocity of the superfluid carriers. If a constant current bias is applied to the bridge, then the velocity of the superfluid carriers will have to increase in order to maintain a constant current density due to the decrease of superfluid carriers in the illuminated region. The resulting acceleration of the superfluid carriers will produce a voltage across the bridge. This can be understood using a simple model where the effect of this voltage on the normal carriers is not considered. Differentiating Eq. (7) with respect to time gives

$$\frac{\partial J_{\text{SC}}}{\partial t}=n_{\text{SC}}e\frac{\partial v_{\text{SC}}}{\partial t}+ev_{\text{SC}}\frac{\partial n_{\text{SC}}}{\partial t}\ . \tag{8}$$

From the condition of constant bias current I, Eq. (8) becomes

$$0=\frac{n_{\text{SC}}e^2}{m}E+J_{\text{SC}}\frac{1}{n_{\text{SC}}}\frac{\partial n_{\text{SC}}}{\partial t}\ , \tag{9}$$

where E is the electric field generated across the bridge by the acceleration of the carriers. The voltage V across the bridge can be found by substituting $E=V/l$ and $J_{\text{SC}}=I/wd$ into Eq. (9) giving

$$\begin{aligned}V&=-I\frac{ml}{e^2wd}\frac{1}{n_{\text{SC}}^2}\frac{\partial n_{\text{SC}}}{\partial t}\\&=I\frac{d}{dt}\left[\frac{ml}{n_{\text{SC}}e^2wd}\right]\\&=I\frac{d}{dt}L_{\text{KIN}}\ ,\end{aligned} \tag{10}$$

where the first form of Eq. (6) has been used for the kinetic inductance. The voltage can be estimated from

$$V_{\text{KIN}}=I\frac{d}{dt}L_{\text{KIN}}\cong I\frac{\Delta L_{\text{KIN}}}{\Delta t}\ , \tag{11}$$

where ΔL_{KIN} is the change in kinetic inductance over some time increment Δt. If $f_{\text{SC initial}}$ and $f_{\text{SC final}}$ are the initial and final superfluid fractions at time t and $t+\Delta t$, respectively, then

$$\Delta L_{\text{KIN}}=\frac{1}{\varepsilon_0\omega_P^2}\left[\frac{l}{wd}\right]\left[\frac{1}{f_{\text{SC final}}}-\frac{1}{f_{\text{SC initial}}}\right]\ . \tag{12}$$

Equation (11) predicts a positive voltage while the superfluid fraction is decreasing followed by a negative voltage as the superfluid density recovers to its initial value. At temperatures close to T_c, Eq. (12) will diverge as $f_{\text{SC final}}$ approaches zero. The resulting divergence of Eq. (11) will not occur if the effect of the normal fluid component is considered in a more complete analysis. Equation (11) also predicts a linear dependence of the photoresponse with bias current. This is exactly what was observed for the fast photoresponse as discussed in Sec. III D and shown in Figs. 7 and 9.

To estimate the magnitude of the voltage generated by changes in kinetic inductance, we use the 260 nm bridge biased at 100 mA as an example. The plasma frequency for YBCO thin films[54] is about 1.67×10^{15} s^{-1} (≈1.1 eV), which gives $\lambda_L(T=0)\approx180$ nm using $\lambda_L(T=0)=c/\omega_P$, where c is the velocity of light. If initially at low temperature so that $f_{\text{SC initial}}\approx1$, then a 10% decrease in superfluid fraction to $f_{\text{SC final}}=0.9$ over the 100 ps time scale of the laser pulse ($l=20$ μm, amplifier voltage gain$=10$) will produce a change in kinetic inductance according to Eq. (12) of about 35 fH and voltage transient using Eq. (11) of about 0.35 mV. If the 30 nm film biased at 15 mA is used as an example, the change in kinetic inductance would be about 150 fH producing a transient voltage of 0.22 mV.

A significant change in the superfluid fraction is possible from heating of the bridge by the laser pulse. For instance, using Eq. (1) for the 260 nm film at 50 K with $C\approx0.49$ J/cm^3 K and $F=100$ μJ/cm^2 gives a temperature transient of about 6.7 K. If f_{SC} varies as $1-(T/T_c)^2$, as measured[55,56] for YBCO thin films, then the superfluid fraction will change from 0.68 to 0.59 ($T_c=89$ K). This is a 13% change in f_{SC}, which is large enough to produce observable transient kinetic inductance signals with a 100 ps laser pulse. A simulation of this process provides estimates for voltage transients well within an order of magnitude of the observed photoresponse, as discussed below.

2. Simulation results

The parameters used in the simulation are given in Table IV. The simulation involved calculating the temperature as a function of time in the 260 nm film as the 100 ps FWHM laser pulse heated the bridge. The change in temperature ΔT as a function of time t was obtained by solving

$$\frac{d\Delta T(t)}{dt}=\frac{G(t)}{C(t,T)}-\frac{\Delta T(t)}{\tau(t,T)}\ , \tag{13}$$

where G is the heat generation term in W/cm^3 and τ is the thermal escape time given by Eq. (2). The generation term was given by

$$G(t)=G_0 e^{-(t/\tau_P)^2}\ , \tag{14}$$

where τ_P is the pulse width term and

$$G_0=\frac{F}{\sqrt{\pi}\,d\,\tau_P}\left[\frac{E_{\rm ABS}}{E_0}\right]\ , \tag{15}$$

so that integrating Eq. (14) over all time gives the total energy absorbed in the bridge per pulse. Figure 15(a) shows the generation term due to the laser pulse and the temperature $T(t)$ in the bridge as a function of time for an initial temperature of 75 K. Figure 15(b) shows the resulting variation in the superfluid fraction as a function of time using a two-fluid model $1-(T/T_c)^2$ dependence of the superfluid fraction. The kinetic inductance of the bridge, calculated from Eq. (6), is also shown in Fig. 15(b). The change in kinetic inductance for each time increment was calculated using Eq. (12), and the voltage generated from this change in kinetic inductance is shown as the dashed line in Fig. 15(c) using Eq. (11) multiplied by the voltage gain AV of the amplifier. The simulation also incorporated an exponential fit to the resistive transition at 100 mA for the 260 nm film shown in Fig. 5. The simulation shows from the dotted line in Fig. 15(c) that the induced temperature transient is large enough to bring the temperature of the bridge far enough into the resistive transition region to give a resistive bolometric response. The total photoresponse is the sum of the kinetic inductance component and the resistive component, which resembles the wave form seen in Fig. 3(c) where a fast voltage transient is followed by a slower response. The simulation shows that the fast component is the kinetic inductive bolometric photoresponse and the slow component is the resistive bolometric photoresponse. The kinetic inductive component is roughly the same width as the incident laser pulse, and does not depend on the slow thermal escape time from the film.

A fit to the heat capacity[46,47] as a function of temperature for YBCO is shown in Fig. 16. Using this fit, the simulation was able to provide values for the maximum amplitude of the temperature change $\Delta T_{\rm MAX\ (Simul.)}$ as a function of temperature in the 260 nm film. Approximate values $\Delta T_{\rm MAX\ (Approx.)}$ obtained from Eq. (1) assuming C is the value for the heat capacity at the initial temperature T provide reasonable estimates of the simulated transient temperatures only above 40 K. Due to the small heat capacity at low temperatures, the transient temperatures below 30 K can be quite high.

Using a $1-(T/T_c)^2$ dependence in the superfluid fraction, the peak voltage response as a function of temperature from the simulation is shown in Fig. 17. Multiplying the observed data points by a factor of 3.5 provides good agreement with the simulation results. Above 70 K, the resistive bolometric component becomes significant and eventually dominates over the kinetic inductive response as the temperature is increased further. Below 70 K, only the fast kinetic inductive component is observed. The simulation provides better than order of magnitude estimates for the temperature variation of the peak photoresponse signal and the onset of the slow resistive component. The factor of 3.5 needed to provide good agreement may be due to uncertainties in the laser fluence and the absorbed energy, in addition to attenuation of the broadband signals in the experimental setup. Simulation results have shown an almost linear dependence of the peak voltage signal as a function of laser fluence from 0

TABLE IV. List of parameter values used in the simulation described in the text. Values for ω_P, δ, R, and $R_{\rm BD}$ were taken from Refs. 54, 49, 48, and 5, respectively.

Parameter	Symbol	Value	Units
Bridge thickness	d	260	nm
Bridge width	w	10	μm
Length of bridge exposed to laser	l	20	μm
Critical temperature	T_c	89	K
Bias current	I	100	mA
Current density	J	3.8×10^6	A/cm^2
Plasma frequency	ω_P	1.67×10^{15}	s^{-1}
Pulse width term for 100 ps FWHM	τ_P	60	ps
Laser fluence	F	100	μJ/cm^2
Optical penetration depth at 532 nm	δ	90	nm
Reflectivity at 532 nm	R	0.1	
Ratio of absorbed to incident energy	$E_{\rm ABS}/E_0$	0.85	
Thermal boundary resistance	$R_{\rm BD}$	1.0×10^{-3}	K cm^2/W
Generation term constant	G_0	3.074×10^{10}	W/cm^3
Amplifier voltage gain	AV	10	

to 150 μJ/cm^2 and in a temperature range from 40 to 70 K. Preliminary observations on a different sample have revealed a linear dependence of the fast photoresponse on laser fluence below 100 μJ/cm^2. The simulation also predicts a fast photoresponse with approximately the same duration as the laser pulse, which means attenuation of the broadband pulses will be independent of temperature. Multiplying the observed results by a temperature independent factor to account for uncertainties in laser fluence and signal attenuation in order to obtain a better fit with the simulation is reasonable. Given the simplicity of the simulation model with no adjustable parameters other than the temperature dependence of the superfluid fraction as discussed below, better than order of magnitude agreement between the observed data and the simulation results is very encouraging.

Recently, Hardy *et al.*[57] showed from microwave

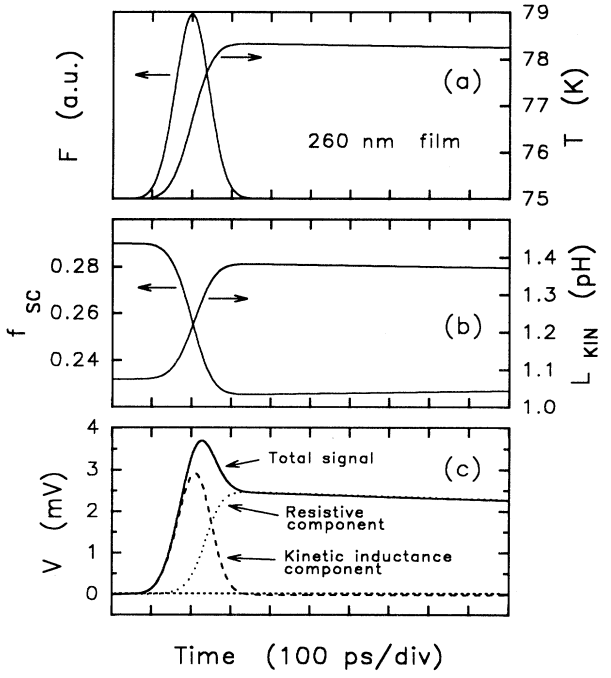

FIG. 15. Simulation results plotted as a function of time for the 260 nm film at a temperature of 75 K, 100 mA bias current, and laser fluence of 100 μJ/cm^2. The parameters used in the simulation are listed in Table IV. The laser pulse intensity F is plotted in (a), which induces a temperature transient T in the bridge. This temperature transient reduces the superfluid fraction f_{SC} which varies as $1-(T/T_c)^2$ in this case, and increases the kinetic inductance L_{KIN} of the bridge, as shown in (b). The increase in kinetic inductance produces a fast voltage transient indicated in (c) as the kinetic inductance component (dashed line). This is also referred to in the text as the kinetic inductive bolometric photoresponse. Since the temperature is within the resistive transition region, a resistive bolometric component (dotted line) is also produced. The total photoresponse signal (solid line), therefore, shows a fast component at the start of a slow component with a decay time determined by the thermal escape time from the film. Similar photoresponse signals were observed at 75 K, as seen in Fig. 3(c).

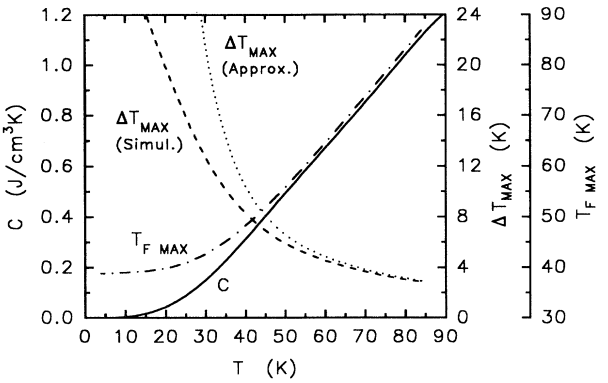

FIG. 16. Heat capacity C as a function of temperature T for YBCO. The plot for C is a fit to heat capacity data taken from Refs. 46 and 47. This heat capacity curve was used in the simulation to determine the temperature transients induced in the film by the laser pulse. For the 260 nm film with a fluence of 100 μJ/cm^2, the maximum temperature transient $\Delta T_{MAX\ (Simul.)}$ from the simulation results can be compared to approximate estimates of the temperature transient $\Delta T_{MAX\ (Approx.)}$ calculated from Eq. (1). The maximum temperature T_{FMAX} reached in the film according to the simulation is also plotted as a function of the initial temperature T of the film, where $T_{FMAX} = T + \Delta T_{MAX\ (Simul.)}$.

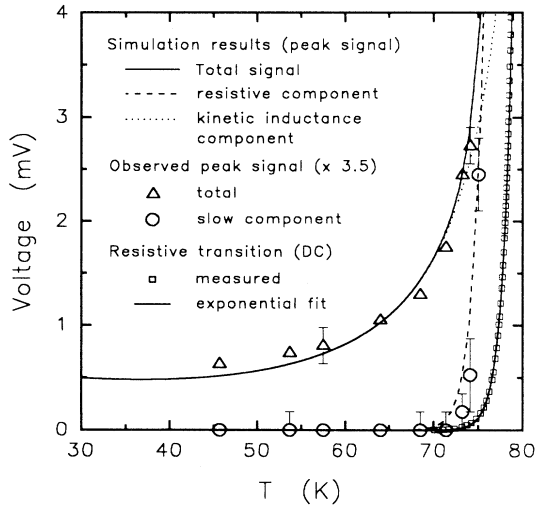

FIG. 17. Comparison of the voltage transient amplitudes obtained from the simulation to the observed peak signals (open triangles) as a function of temperature for the 260 nm film. The parameters used in the simulation are shown in Table IV. In this case, the simulation used a $1-(T/T_c)^2$ dependence of the superfluid fraction with temperature. The observed data values have been multiplied by a factor of 3.5 to obtain a reasonable fit to the simulation results. The rapid increase in the amplitude of the observed slow component (open circles) above 70 K coincides with the simulation results for the amplitude of the resistive component (dashed line). The amplitude of the kinetic inductance component (dotted line) is seen to fall below the peak signal amplitude (solid line) for temperatures above 70 K where the resistive component begins to take over. The measured resistive transition across the bridge (open squares) is shown with the exponential fit (solid line through the squares) used to determine the resistive photoresponse in the simulation.

penetration depth measurements that the superfluid fraction varied linearly at low temperatures for high-quality single crystals of YBCO. This is plotted in Fig. 18 along with $1-t^2$, $1-t^4$, and BCS[58] temperature dependencies of the superfluid fraction where $t=T/T_c$ is the reduced temperature. Figure 19 compares the observed data to the simulation results using each of the superfluid fraction curves from Fig. 18. Only a factor of 2 is needed to get the observed data in good agreement with the simulation results using the superfluid fraction determined by Hardy *et al.*[57] Both the $1-t^2$ and BCS dependencies give similar results above 50 K, but at lower temperatures the BCS curve falls below the $1-t^2$ fit. At this stage, the $1-t^4$ curve is incompatible with the data, however, extending the photoresponse measurements to lower temperatures would help to differentiate between the various dependencies.

The model used in the simulation for the origin of the fast photoresponse provides good agreement with the observed data, but several approximations and assumptions were made. The expression for kinetic inductance in Eq. (6) assumes the current distribution in the superconducting bridge is uniform. At microwave frequencies this is not the case, and many studies have been done[38,56,59] which look at the effect of current distribution on the kinetic inductance of microstrip transmission lines. Attenuation of the kinetic inductive voltage transient by the normal fluid component in the superconductor was considered in a separate simulation, but was found to be insignificant with normal carrier relaxation times shorter than 1 ps. A decrease in the peak amplitude was seen for relaxation times longer than 10 ps. Relaxation times longer than 10 ps will occur[55] at temperatures below about 40 K, but the decrease in normal fluid fraction will reduce the attenuation by the normal component.

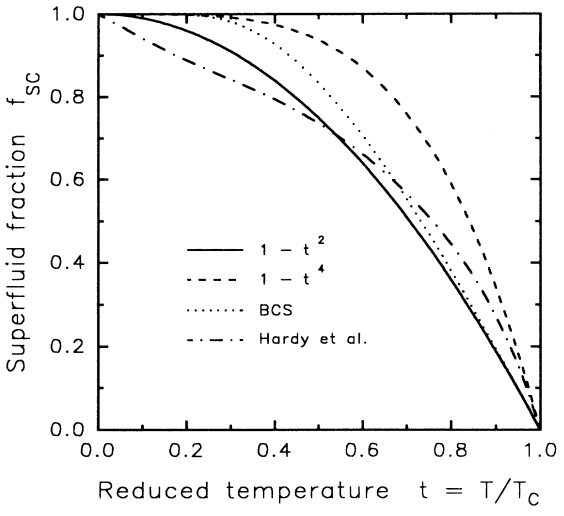

FIG. 18. Theoretical superfluid fraction f_{SC} as a function of reduced temperature $t=T/T_c$ for the following temperature dependencies: $1-t^2$ (solid line), $1-t^4$ (dashed line), BCS variation from Ref. 58 (dotted line), and as observed in YBCO single crystals by Hardy *et al.* from Ref. 57 (dash-dot line). Each of these superfluid fraction curves were used by the simulation to see which gave the best fit to the temperature dependence of the observed photoresponse data, as shown in Fig. 19.

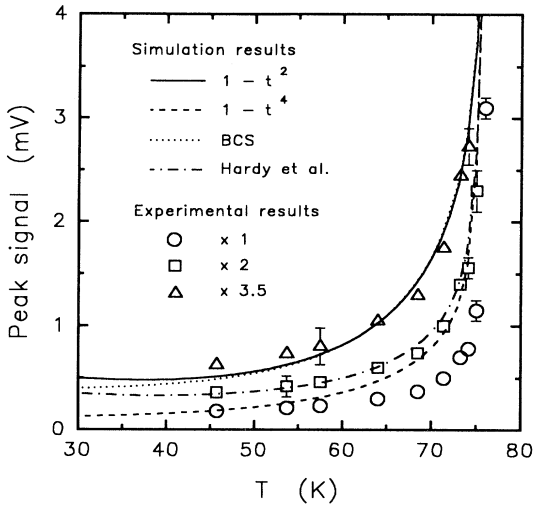

FIG. 19. Comparison of the peak signals obtained from the simulation results to those observed experimentally as a function of temperature for the 260 nm film. The simulation results for the peak signal amplitudes consist of four curves which use superfluid fractions (Fig. 18) varying as $1-t^2$ (solid line), $1-t^4$ (dashed line), BCS behavior from Ref. 58 (dotted line), and as observed by Hardy *et al.* in Ref. 57 for YBCO signal crystals (dot-dash line). The observed data (open circles) is multiplied by factors of 2 (open squares) and 3.5 (open triangles) to see which superfluid fraction variation used in the simulation gives the best fit.

The model also assumes uniform heating over the entire thickness of the bridge. This is clearly not the case for optically thick films, while for thinner films uniform heating is a reasonable approximation. It was also assumed that the optical penetration depth was relatively insensitive to temperature, which has been observed elsewhere[60] for transmittance measurements through 180 nm YBCO films between 10 and 300 K. The simulation only considered thermal escape times governed by thermal boundary resistance as described by Eq. (2) and did not take into account the effects of thermal diffusion times given by Eq. (5). The thermal boundary resistance was also assumed to be constant over the entire temperature range. This is true from 90 to 200 K,[5] but as discussed in Sec. III E in Eq. (4), R_{BD} will probably increase at temperatures below 30 K. This will increase the thermal escape time from the film which will tend to increase the signal amplitudes obtained from the simulation but will not affect the speed of the kinetic inductive response.

Uncertainties in laser spot size on the bridge and the energy in each pulse will affect the value for the laser fluence used in the simulation. The simulation approximated the Gaussian profile of the laser spot with a uniform fluence over an effective spot size. Finally, the value for the plasma frequency[54] of 1.67×10^{15} s^{-1} (1.1 eV) was obtained from far infrared measurements on similar YBCO films. Variations in sample quality may change

ω_P, thereby affecting the signal amplitude.

A further test of the validity of the kinetic inductive bolometric photoresponse model used to interpret the fast component in the observed wave forms is the prediction by Eq. (11) of negative voltage transients. Simulation results for the 30 nm film at 54 K with 20 mA bias are shown in Fig. 20. Figure 21 shows the simulation results for the 130 nm film at 61 K and 100 mA bias. Once the laser pulse has stopped heating the film, the films relax to their original starting temperatures at a rate determined by the thermal escape time. This can be seen by the faster decay time of the temperature transient in Fig. 20(a) for the 30 nm film compared to the slower decay in Fig. 21(a) for the 130 nm film. The resulting faster rate of increase in the superfluid fraction for the 30 nm film seen in Fig. 20(b) gives rise to a negative voltage transient in Fig. 20(c) a little less than 0.2 mV (≈ -0.14 mV). The negative voltage transient for the 130 nm film in Fig. 21(c) is hardly visible (≈ -0.024 mV) because the rate at which Cooper pairs reform as the heat escapes from the film is too slow.

Figure 22 shows fast photoresponse wave forms taken from the 30 and 130 nm films under operating conditions identical to those used in the simulation results of Figs. 20 and 21. Wave forms with approximately the same amplitude were chosen to make sure any negative transients were not due to spurious circuit effects. The photoresponse observed for the 30 nm film in Fig. 22(a)

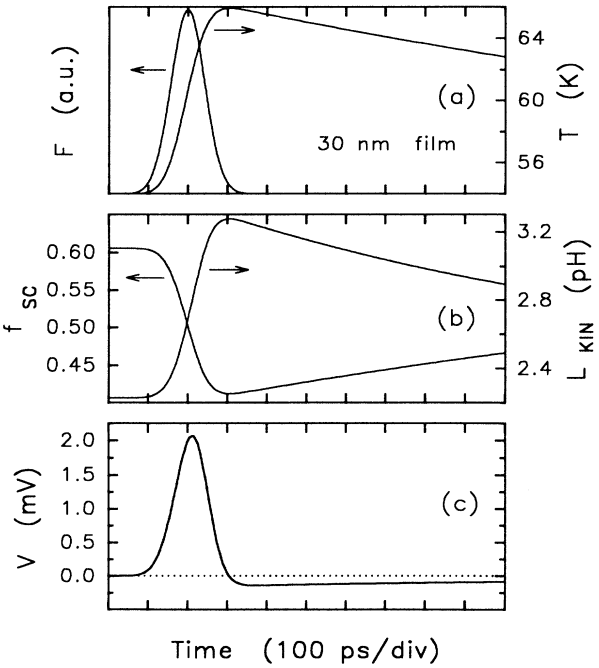

FIG. 20. Simulation results for the 30 nm film at a temperature of 54 K and a bias current of 20 mA. The film is biased below its resistive transition region, so only the kinetic inductive bolometric response appears in the simulation. Notice the negative voltage transient in (c) produced once the superfluid fraction in (b) starts to increase again and the kinetic inductance begins to drop.

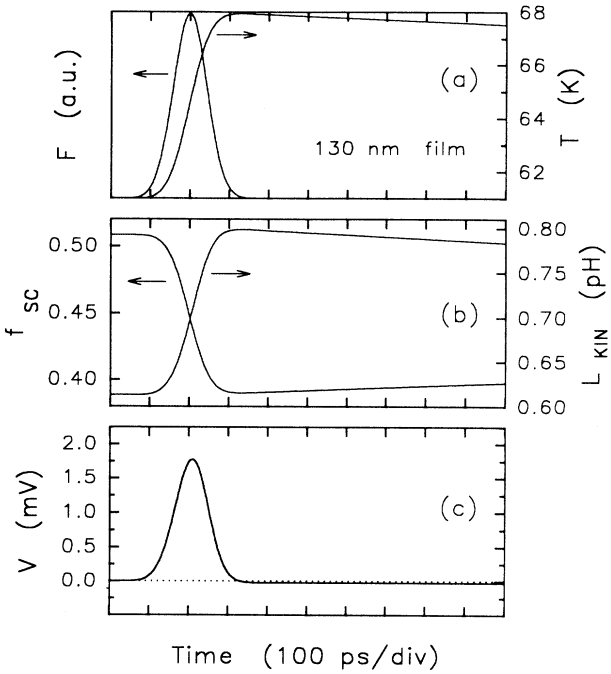

FIG. 21. Simulation results for the 130 nm film at a temperature of 61 K and a bias current of 100 mA. The film is biased below its resistive transition region, so only the kinetic inductive bolometric response appears in the simulation. Notice that the negative voltage transient in (c) produced once the superfluid fraction in (b) starts to increase again is much less than the negative transient expected from the 30 nm film shown in Fig. 20(c). This is because the thermal decay time in (a) is much slower than that for the 30 nm film seen in Fig. 20(a). The superfluid fraction takes longer to recover to its initial value than for the 30 nm film, which results in a slower change in L_{KIN} and a smaller negative voltage.

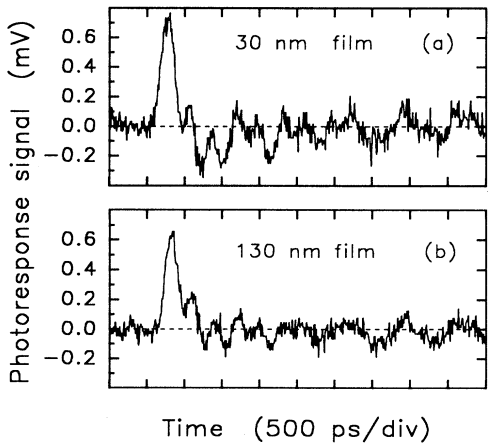

FIG. 22. Fast photoresponse signals observed from the (a) 30 nm and (b) 130 nm films. The 30 nm film was at a temperature of 54 K and biased at 20 mA. The signal from the 130 nm film was taken at 61 K and 100 mA. Both films were biased below their resistive transition regions. A small, negative transient is observed for the 30 nm film in (a) but not for the 130 nm film in (b). This is consistent with the simulation results shown in Figs. 20 and 21. Note the difference in time scale with Figs. 20 and 21.

shows a slight negative voltage transient less than 0.2 mV in amplitude, whereas no negative voltage transient is discernable in Fig. 22(b) for the 130 nm film. Notice that the oscilloscope noise is relatively flat before the transients are seen in Fig. 22. The increased noise seen after the fast transient is due to ringing and reflections of the fast voltage transient at the sample. The negative transient in Fig. 22(a) is seen as a negative-going trend in the average value of these oscillations, lasting about 1 ns after the fast positive-going pulse. A 60 nm film also exhibited a small negative voltage transient. As seen in Fig. 4(b), no negative voltage transient was observed for the 260 nm film. Figure 10(c) for the 30 nm film at a slightly smaller bias than that used in Fig. 22(b) also shows a small negative transient. The observation of negative voltage transients only in very thin films with faster thermal escape times supports the kinetic inductive bolometric photoresponse mechanism we are proposing for the origin of the fast photoresponse in YBCO thin films.

3. *Possibility of nonequilibrium effects*

In our simulation, we assumed that the distribution of quasiparticles was in equilibrium with the local temperature of the lattice. Of course, if a sufficiently short laser pulse is used to excite the superconductor, then this condition would not be initially satisfied. The nonbolometric kinetic inductive photoresponse that would then arise[16,18–20,23,25] might be identified by deviations from the simulated kinetic inductive bolometric response. This would provide insight into the complex quasiparticle dynamics and relaxation processes. Several authors have suggested that a single photon could be responsible for breaking many Cooper pairs due to impact ionization and emission of optical phonons which subsequently break more Cooper pairs.[18,32] Estimates based on conservation of energy have suggested[32] that as many as 100 Cooper pairs can be broken by a single optical photon. We note that these estimates are based on a minimum quasiparticle energy comparable to the BCS "*s*-wave" gap, and that any gap structure with nodes could lead to multiplication factors much higher than 100.

Pump-probe results suggest that during a 100 ps pulse the quasiparticles will be in equilibrium with the lattice temperature. The duration of the quasiparticle thermalization process has been measured in YBCO thin films[32] to be about 350 fs, and recombination back into Cooper pairs was believed to be complete after 5 ps.[32]

Suppression of the superconducting order parameter by the excess quasiparticle distribution has also been proposed as a nonbolometric mechanism and origin of the fast photoresponse in YBCO thin films.[16–18,20,22–24,33] If the gap is sufficiently suppressed, the critical current will be exceeded and the superconductor will enter a resistive state.[18,20] Signatures of this mechanism would be a nonlinear current dependence at threshold and a resistive rather than inductive signal. Whether this occurs with subpicosecond laser pulses is still unclear. The fact that the photoresponse was linear with bias current provides evidence that nonequilibrium gap suppression was probably not involved in our experiments.

4. *Possibility of photoactivated flux flow*

Laser-induced depinning of vortices has been proposed[17,29] as a mechanism for the fast photoresponse. Once the vortices have been freed, they move with a velocity governed by the Lorentz force generated by the current density J and the viscosity η for flux flow in the film. It is the motion of these photoactivated vortices perpendicular to the current which produces a voltage drop across the superconducting bridge. We now try to estimate the size of this effect for the 260 nm film.

Since no external fields have been applied, the only source of vortices is from the self-field of the current-carrying bridge. The current density and resulting magnetic field are peaked near the edges of the bridge.[61] The peak amplitude of the self-field at the edge of a 10 μm wide superconducting bridge has been calculated[61] to be about 190 G using a penetration depth of 220 nm and a current density of 10^7 A/cm^2. In a simple model, if one assumes that the laser pulse is able to activate the movement of a uniform magnetic field B of 100 G at a current density J of 5×10^6 A/cm^2 over a length l of 20 μm, then the flux flow voltage will be given by $V=Blv$, where v is the flux flow velocity. Using $v=J\phi_0/\eta$, where ϕ_0 is the flux quantum and $\eta\approx2\times10^{-7}$ N s/m^2 at 50 K for YBCO thin films,[62] the flux flow voltage would be about 1 mV after amplification with the $\times10$ amplifier. This is certainly within the correct order of magnitude of the observed fast photoresponse, but such a mechanism cannot account for the origin of the fast photoresponse. In the flux flow model, $v\sim J$ and $B\sim J$ making $V\sim J^2$. Furthermore, if the activation energy for depinning of vortices decreases with increasing current[29] then the photoresponse should increase even faster than J^2. This disagrees with the observed linear dependence of the fast photoresponse with the bias current. An external magnetic field of 100 G was applied perpendicular to the bridge of a different sample in experiments[28] similar to the ones described here, but no change in the amplitude of the fast photoresponse was observed implying the absence of photoactivated flux flow.

IV. SUMMARY

We have measured the photoresponse from current biased YBCO bridge structures exposed to 100 ps laser pulses in films ranging in thickness from 30 to 260 nm. Near the resistive transition, the photoresponse consisted of a fast component less than 500 ps wide followed by a slower component with a decay of several nanoseconds. Well below the resistive transition, only the fast component was observed which persisted to low temperatures. We have shown that the slow component is due to a resistive bolometric response where the laser pulse heats the film into the resistive transition region. The decay of the slow component is therefore determined by the thermal escape time from the film, which is faster for thinner films in agreement with predicted results. The

fast component is consistent with a kinetic inductive bolometric response. Heating from the laser pulse decreases the superfluid fraction in the superconductor which in turn increases the kinetic inductance of the bridge. This gives rise to a positive transient voltage which has the same width as the incident laser pulse. Fast transients were observed in both thin (30 nm) films and thick (260 nm) films. Negative voltage transients were only seen in the thinnest films where the thermal escape times were the fastest. This offers the possibility of using the amplitudes and decay times of the negative transients to estimate thermal escape times and thus the thermal boundary resistance as a function of temperature below T_c in thin films. The origin of the fast photoresponse of YBCO epitaxial thin films is therefore bolometric in nature over the duration of the 100 ps laser pulse, and arises from thermally induced changes in the kinetic inductance of the current-biased bridge. The observed linear dependence of the fast photoresponse with bias current is consistent with this mechanism.

A simulation based on the kinetic inductive bolometric response model provided reasonable agreement with the temperature dependence of the observed photoresponse data. Nonequilibrium or nonbolometric mechanisms were not required to explain the origin of the fast component. The only adjustable parameter in the simulation was the temperature dependence of the superfluid fraction. The simulation also provided a comparison between the various postulated temperature dependencies of the superfluid fraction in YBCO, but data at lower temperatures is required to determine the best fit.

Improvements in the electrical bandwidth of the photoresponse setup will be necessary in order to resolve the fast voltage transients. This will provide more accurate measurements of the amplitudes of the photoresponse signals for comparison with the simulation results. Since the amplitude of the positive portion of the kinetic inductive bolometric signal relies on the rate at which the laser pulse heats the film, shorter laser pulses should produce larger and faster voltage transients which could have interesting implications in the development of high speed optical detectors made from high-T_c superconductors.

ACKNOWLEDGMENTS

We would like to thank R. Hughes, A. McConnel, and T. Strach for their assistance with the film growth and for providing some of the laser ablated films. We are grateful for many useful discussions with T. Timusk regarding the plasma frequency and other optical properties of YBCO thin films. This work was supported by the Ontario Centre for Materials Research and the Natural Sciences and Engineering Research Council of Canada.

[1]P. L. Richards, J. Clarke, R. Leoni, Ph. Lerch, S. Verghese, M. R. Beasley, T. H. Geballe, R. H. Hammond, P. Rosenthal, and S. R. Spielman, Appl. Phys. Lett. **54**, 283 (1989).

[2]Q. Hu and P. L. Richards, Appl. Phys. Lett. **55**, 2444 (1989).

[3]S. Verghese, P. L. Richards, K. Char, D. K. Fork, and T. H. Geballe, J. Appl. Phys. **71**, 2491 (1992).

[4]S. Verghese, P. L. Richards, D. K. Fork, K. Char, and T. H. Geballe, IEEE Trans. Appl. Superconductivity **3**, 2115 (1993).

[5]M. Nahum, S. Verghese, P. L. Richards, and K. Char, Appl. Phys. Lett. **59**, 2034 (1991).

[6]Advanced Fuel Research, 87 Church Street, East Hartford, CT 06108 (unpublished). Specifications: Response from near IR to the far IR, 10 kHz thermal response speed, 10 000 V/W responsivity, NEP $< 10^{-11}$ W/Hz$^{1/2}$, and $D^* > 10^{10}$ cm Hz$^{1/2}$/W. See also Q. Li, D. B. Fenner, W. D. Hamblen, and D. G. Hamblen, Appl. Phys. Lett. **62**, 2428 (1993).

[7]J. C. Culbertson, U. Strom, S. A. Wolf, and W. W. Fuller, Phys. Rev. B **44**, 9609 (1991).

[8]M. G. Forrester, M. Gottlieb, J. R. Gavaler, and A. I. Braginski, IEEE Trans. Magn. **MAG-25**, 1327 (1989).

[9]Y. Enomoto, T. Murakami, and M. Suzuki, Physica C **153-155**, 1592 (1988).

[10]G. Schneider, H. Lengfellner, J. Betz, K. F. Renk, and W. Prettl, Int. J. IR MM Waves **12**, 1 (1991).

[11]E. M. Gershenzon, G. N. Gol'tsman, A. D. Semenov, and A. V. Sergeev, IEEE Trans. Magn. **MAG-27**, 1321 (1991).

[12]M. G. Forrester, M. Gottlieb, J. R. Gavaler, and A. I. Braginski, Appl. Phys. Lett. **53**, 1332 (1988).

[13]W. S. Brocklesby, D. Monroe, A. F. J. Levi, M. Hong, S. H. Liou, J. Kwo, C. E. Rice, P. M. Mankiewich, and R. E. Howard, Appl. Phys. Lett. **54**, 1175 (1989).

[14]G. L. Carr, M. Quijada, D. B. Tanner, C. J. Hirschmugl, G. P. Williams, S. Etemad, B. Dutta, F. DeRosa, A. Inam, T. Venkatesan, and X. Xi, Appl. Phys. Lett. **57**, 2725 (1990).

[15]H. S. Kwok, J. P. Zheng, Q. Y. Ying, and R. Rao, Appl. Phys. Lett. **54**, 2473 (1989).

[16]L. Shi, G. L. Huang, C. Lehane, J. P. Zheng, and H. S. Kwok, Appl. Phys. Lett. **61**, 489 (1992).

[17]A. Frenkel, M. A. Saifi, T. Venkatesan, P. England, X. D. Wu, and A. Inam, J. Appl. Phys. **67**, 3054 (1990).

[18]N. Bluzer, Phys. Rev. B **44**, 10 222 (1991).

[19]N. Bluzer, J. Appl. Phys. **71**, 1336 (1992).

[20]N. Bluzer, IEEE Trans. Appl. Superconductivity **3**, 2869 (1993).

[21]M. Johnson, Appl. Phys. Lett. **59**, 1371 (1991).

[22]A. D. Semenov, G. N. Gol'tsman, I. G. Gogidze, A. V. Sergeev, E. M. Gershenzon, P. T. Lang, and K. F. Renk, Appl. Phys. Lett. **60**, 903 (1992).

[23]A. D. Semenov, I. G. Goghidze, G. N. Gol'tsman, A. V. Sergeev, E. E. Aksaev, and E. M. Gershenzon, IEEE Trans. Appl. Superconductivity **3**, 2132 (1993).

[24]R. S. Nebosis, M. A. Heusinger, W. Schatz, K. F. Renk, G. N. Gol'tsman, B. S. Karasik, A. D. Semenov, and G. M. Gershenzon, IEEE Trans. Appl. Superconductivity **3**, 2160 (1993).

[25]A. Ghis, S. Pfister, J. C. Villegier, M. Nail, and J. P. Maneval, IEEE Trans. Appl. Superconductivity **3**, 2136 (1993).

[26]M. I. Flik, P. E. Phelan, and C. L. Tien, Cryogenics **30**, 1118 (1990).

[27]S. Zeuner, H. Lengfellner, J. Betz, K. F. Renk, and W. Prettl, Appl. Phys. Lett. **61**, 973 (1992).

[28]F. A. Hegmann and J. S. Preston, Appl. Phys. Lett. **62**, 1158 (1993).

[29]E. Zeldov, N. M. Amer, G. Koren, A. Gupta, R. J. Gambino,

and M. W. McElfresh, Phys. Rev. Lett. **62**, 3093 (1989); E. Zeldov, N. M. Amer, G. Koren, and A. Gupta, Phys. Rev. B **39**, 9712 (1989).

[30]A. M. Kadin, M. Leung, A. D. Smith, and J. M. Murduck, Appl. Phys. Lett. **57**, 2847 (1990).

[31]W. R. Donaldson, A. M. Kadin, P. H. Ballentine, and R. Sobolewski, Appl. Phys. Lett. **54**, 2470 (1989). A. M. Kadin, P. H. Ballentine, and W. R. Donaldson, Physica B **165&166**, 1507 (1990).

[32]S. G. Han, Z. V. Vardeny, K. S. Wong, O. G. Symko, and G. Koren, Phys. Rev. Lett. **65**, 2708 (1990).

[33]G. L. Eesley, J. Heremans, M. S. Meyer, G. L. Doll, and S. H. Liou, Phys. Rev. Lett. **65**, 3445 (1990).

[34]J. M. Chwalek, C. Uher, J. F. Whitaker, G. A. Mourou, J. Agostinelli, and M. Lelental, Appl. Phys. Lett. **57**, 1696 (1990).

[35]T. Gong, L. X. Zheng, W. Xiong, W. Kula, Y. Kostoulas, R. Sobolewski, and P. M. Fauchet, Phys. Rev. B **47**, 14 495 (1993).

[36]S. D. Brorson, A. Kazeroonian, D. W. Face, T. K. Cheng, G. L. Doll, M. S. Dresselhaus, G. Dresselhaus, E. P. Ippen, T. Venkatesan, X. D. Wu, and A. Inam, Solid State Commun. **74**, 1305 (1990); S. D. Brorson, A. Kazeroonian, J. S. Moodera, D. W. Face, T. K. Cheng, E. P. Ippen, M. S. Dresselhaus, and G. Dresselhaus, Phys. Rev. Lett. **18**, 2172 (1990).

[37]S. G. Han, Z. V. Vardeny, O. G. Symko, and G. Koren, Phys. Rev. Lett. **67**, 1053 (1991); G. L. Esley, J. Heremans, M. S. Meyer, and G. L. Doll, *ibid.* **67**, 1054 (1991).

[38]J. M. Pond, J. H. Claassen, and W. L. Carter, IEEE Trans. Microwave Theory and Techniques **MTT-35**, 1256 (1987); W. H. Chang, Appl. Phys. Lett. **50**, 8129 (1979); R. Meservey and P. M. Tedrow, J. Appl. Phys. **40**, 2028 (1969).

[39]B. W. Langley, S. M. Anlage, R. F. W. Pease, and M. R. Beasley, Rev. Sci. Instrum. **62**, 1801 (1991); J. M. Pond, K. R. Carroll, J. S. Horwitz, and D. B. Chrisey, IEEE Trans. Appl. Superconductivity **3**, 1438 (1993).

[40]J. M. Pond, J. H. Claassen, and W. L. Carter, IEEE Trans. Magn. **MAG-23**, 903 (1987); G. K. G. Hohenwarter, J. S. Martens, J. B. Beyer, J. E. Nordman, and D. P. McGinnis, *ibid.* **MAG-25**, 1100 (1989).

[41]E. K. Track, R. E. Drake, and G. K. G. Hohenwarter, IEEE Trans. Appl. Superconductivity **3**, 2899 (1993).

[42]J. E. Sauvageau, D. G. McDonald, and E. N. Grossman, IEEE Trans. Magn. **MAG-27**, 2757 (1991); E. N. Grossman, D. G. McDonald, and J. E. Sauvageau, *ibid.* **MAG-27**, 2677 (1991); J. E. Sauvageau and D. G. McDonald, *ibid.* **MAG-25**, 1331 (1989); D. G. McDonald, Appl. Phys. Lett. **50**, 775 (1987).

[43]R. Kumar, S. K. Malik, S. P. Pai, P. R. Apte, R. Pinto, and R. Vijayaraghavan, Phys. Rev. B **46**, 5766 (1992); S. Tahara, S. M. Anlage, J. Halbritter, C. B. Eom, D. K. Fork, T. H. Geballe, and M. R. Beasley, *ibid.* **41**, 11 203 (1990).

[44]A. Frenkel, E. Clausen, C. C. Chang, T. Venkatesan, P. S. D. Lin, X. D. Wu, A. Inam, and B. Lalevic, Appl. Phys. Lett. **55**, 911 (1989).

[45]D. Gupta, W. R. Donaldson, K. Kortkamp, and A. M. Kadin, IEEE Trans. Appl. Superconductivity **3**, 2895 (1993).

[46]T. Atake, A. Honda, and H. Kawaji, Physica C **190**, 70 (1991).

[47]D. Sanchez, A. Junod, J.-Y. Genoud, T. Graf, and J. Muller, Physica C **200**, 1 (1992).

[48]A. Zibold, K. Widder, H. P. Geserich, T. Scherer, P. Marienhoff, M. Neuhaus, W. Jutzi, A. Erb, and G. Muller-Vogt, Appl. Phys. Lett. **61**, 345 (1992); S. L. Cooper, D. Reznik, A. Kotz, M. A. Karlow, R. Liu, M. V. Klein, W. C. Lee, J. Giapintzakis, D. M. Ginsberg, B. W. Veal, and A. P. Paulikas, Phys. Rev. B **47**, 8233 (1993).

[49]H. Yasuoka, H. Mazaki, T. Terashima, and Y. Bando, Physica C **175**, 192 (1991).

[50]I. Bozovic, Phys. Rev. B **42**, 1969 (1990).

[51]C. D. Marshall, A. Tokmakoff, I. M. Fishman, C. B. Eom, J. M. Phillips, and M. D. Fayer, J. Appl. Phys. **73**, 850 (1993).

[52]S. D. Peacor, R. A. Richardson, F. Nori, and C. Uher, Phys. Rev. B **44**, 9508 (1991); J. L. Cohn, S. A. Wolf, T. A. Vanderah, V. Selvamanickam, and K. Salama, Physica C **192**, 435 (1992).

[53]S. J. Hagen, Z. Z. Wang, and N. P. Ong, Phys. Rev. B **40**, 9389 (1989); Sera, S. Shamoto, M. Sato, I. Watanabe, S. Nakashima, and K. Kumagai, Solid State Commun. **74**, 951 (1990).

[54]T. Timusk (private communication).

[55]D. A. Bonn, R. Liang, T. M. Riseman, D. J. Baar, D. C. Morgan, K. Zhang, P. Dosanjh, T. L. Duty, A. MacFarlane, G. D. Morris, J. H. Brewer, W. N. Hardy, C. Kallin, and A. J. Berlinsky, Phys. Rev. B **47**, 11 314 (1993).

[56]J.-Y. Lee and T. R. Lemberger, Appl. Phys. Lett. **62**, 2419 (1993).

[57]W. N. Hardy, D. A. Bonn, D. C. Morgan, R. Liang, and K. Zhang, Phys. Rev. Lett. **70**, 3999 (1993).

[58]B. Muhlschlegal, Z. Phys. **155**, 313 (1959).

[59]J. W. Baker, J. D. Lejeune, and D. G. Naugle, J. Appl. Phys. **45**, 5043 (1974).

[60]I. Bozovic, D. Kirillov, A. Kapitulnik, K. Char, M. R. Hahn, M. R. Beasley, T. H. Geballe, Y. H. Kim, and A. J. Heeger, Phys. Rev. Lett. **59**, 2219 (1987).

[61]T. R. Lemberger, in *Physical Properties of High Temperature Superconductors III,* edited by D. M. Ginsberg (World Scientific, Singapore, 1992), p. 490.

[62]M. S. Pambianchi, D. H. Wu, L. Ganapathi, and S. M. Anlage, IEEE Trans. Appl. Superconductivity **3**, 2774 (1993).